Nuclear Physics B 368 (1992) 390–412
North-Holland

NUCLEAR
PHYSICS B

The eigenvalue spectra in Z(2) ⊗ Z(2) and SU(2) ⊗ SU(2) fermion–Higgs models *

Ian Barbour [1,2], Wolfgang Bock [2,3], Christine Davies [1], Asit K. De [2,3], David Henty [1], Jan Smit [4] and Thomas Trappenberg [2,3]

[1] *Department of Physics and Astronomy, University of Glasgow, Glasgow, G12 8QQ, UK*
[2] *HLRZ c/o KFA Jülich, P.O. Box 1913, D-5170 Jülich, Germany*
[3] *Institut für Theoretische Physik E, RWTH Aachen, D-5100 Aachen, Germany*
[4] *Institute of Theoretical Physics, Valckenierstraat 65, NL-1018 XE Amsterdam, The Netherlands*

Received 28 August 1990
(Revised 5 August 1991)
Accepted for publication 27 August 1991

We present an analysis of the eigenvalue spectra of the Dirac operator M and related operators M' and $M^{\dagger}M$ in an SU(2)⊗SU(2) and a Z(2)⊗Z(2) fermion–Higgs model in the quenched approximation. We especially study the spectra in the symmetric and broken symmetry phases along the crossover line which was recently discovered in these models in numerical simulations. It turns out that in the symmetric phases of both models zero modes emerge along the crossover line. In the case of the Z(2) model the zero modes follow the crossover line into the broken symmetry phase whereas in the case of the SU(2) model they appear to stop at the phase transition line between the symmetric and the broken phases.

1. Introduction

Non-perturbative understanding of the spontaneous symmetry breaking in the standard model of electroweak interactions has been the subject of many recent investigations. Studies of lattice regularized pure scalar Φ^4 theory have been able to confirm the perturbative picture of triviality and have determined an upper bound on the Higgs mass (for recent reviews see refs. [1–3] and references therein). The next stage of the calculation naturally involves the so-called Yukawa models on the lattice involving both scalar and fermion fields interacting through Yukawa couplings. Initial studies have considered scalar–fermion models on the lattice with Z(2), U(1) and SU(2) symmetries. For reviews see refs. [4–6] and references therein.

The non-perturbative investigations of the lattice Yukawa models have revealed a variety of interesting and unusual properties. At intermediate values of the

* Supported by the Deutsche Forschungsgemeinschaft, the Stichting voor Fundamenteel Onderzoek der Materie (FOM) and the UK SERC.

Yukawa coupling there exists a region which the fermionic observables are very sensitive to [7,8]. Let us call it the *crossover* region. Across the crossover the behaviour of the fermion mass changes, as explained below. For smaller Yukawa couplings, perturbative expectations about fermion mass generation are fulfilled. For Yukawa couplings above the value corresponding to the crossover there exists, on the contrary, a symmetric phase where the fermions are massive and a broken phase where the fermion mass increases as the vacuum expectation value of the scalar field decreases. For such strong Yukawa couplings, the fermion mass does not notice the phase transition between the symmetric and the broken phase and decouples in the continuum limit. Nevertheless, it has been proposed [9] that using a second derivative Yukawa coupling known as the Wilson–Yukawa coupling [10] which is chirally invariant, this apparently unphysical region may come to use in decoupling species doublers of chirally coupled fermions on the lattice while the masses of the physical fermions can scale. The decoupling of the fermion doublers by making them heavy and scaling of the physical fermion masses have now been demonstrated in these theories using both analytic and numerical techniques [11–17]. Although it is very unclear at the moment what kind of a theory emerges in the continuum limit using the Wilson–Yukawa approach [13,18], from the point of view of understanding Yukawa couplings alone non-perturbatively, investigations on curious phenomena like the crossover would be very valuable.

In this paper we study the eigenmodes of the fermion matrix in the vicinity of the crossover. The peculiarities of the crossover, e.g. the failure or at least a great difficulty to invert the fermion matrix at and around the crossover, can be studied in a more quantitative and direct way in this approach. In particular, we would like to make definite statements about the existence of zero eigenvalues even in the limit of infinite lattice volume. Analogous studies of the eigenmodes in other field theories which involve fermions, such as QCD and QED, have proved useful [19–22]. Details of the quality of the lattice approximation for fermions can also be judged from the spectra [16,23].

We investigate two different lattice Yukawa models in the quenched approximation. One is with the discrete symmetry group $Z(2) \otimes Z(2)$ and the other with the continuous symmetry $SU(2) \otimes SU(2)$. The Z(2) model uses staggered lattice fermions. The SU(2) model is studied both with and without the above-mentioned Wilson–Yukawa coupling.

After defining the two models in sect. 2 we briefly describe in sect. 3 the Lanczos algorithm used to obtain the eigenvalues of the fermion matrices M, $M^\dagger M$ and the related matrix M'. In sect. 4 we describe the eigenvalue spectra of the fermion matrices M and M' in different regions of the phase diagrams for the two models and discuss the appearance of small eigenvalues. In order to obtain information about the volume dependence of the small eigenvalues of M we analyse in sect. 5 the small eigenvalues of the hermitian operator $M^\dagger M$ which allows us to use larger lattices. In sect. 6 we discuss fermion condensates calculated

from the eigenvalues and show in sect. 7 that an effective free fermion mass calculated from the fermion condensate surprisingly has reasonable qualitative behaviour.

2. The models

The models under consideration are defined by the following actions on an euclidean lattice. The Z(2) model with staggered fermions and on-site Yukawa coupling is defined by the action

$$S = S_{\mathrm{H}} + S_{\mathrm{F}},$$

$$S_{\mathrm{H}} = -2\kappa \sum_{x\mu} \phi_x \phi_{x+\hat{\mu}}, \tag{2.1}$$

$$S_{\mathrm{F}} = \bar{\chi} M \chi$$

$$= \sum_{x\mu} \tfrac{1}{2} \eta_{\mu x} \bar{\chi}_x (\chi_{x+\hat{\mu}} - \chi_{x-\hat{\mu}}) + y \sum_x \phi_x \bar{\chi}_x \chi_x, \tag{2.2}$$

where $\eta_{\mu x} = (-1)^{x_1 + x_2 + \cdots + x_{\mu-1}}$, and χ_x and $\bar{\chi}_x$ denote the staggered fermion fields. The action for the SU(2) model is given by

$$S = S_{\mathrm{H}} + S_{\mathrm{F}},$$

$$S_{\mathrm{H}} = -\kappa \sum_{x\mu} \tfrac{1}{2} \mathrm{Tr}\left(\Phi_x^\dagger \Phi_{x+\hat{\mu}} + \Phi_x^\dagger \Phi_{x-\hat{\mu}} \right), \tag{2.3}$$

$$S_{\mathrm{F}} = \bar{\Psi} M \Psi$$

$$= \sum_{x\mu} \tfrac{1}{2} \bar{\Psi}_x \gamma_\mu \left(\Psi_{x+\hat{\mu}} - \Psi_{x-\hat{\mu}} \right) + y \sum_x \bar{\Psi}_x \left(\Phi_x P_{\mathrm{R}} + \Phi_x^\dagger P_{\mathrm{L}} \right) \Psi_x$$

$$+ w \sum_{x\mu} \Big\{ \bar{\Psi}_x \left(\Phi_x P_{\mathrm{R}} + \Phi_x^\dagger P_{\mathrm{L}} \right) \Psi_x$$

$$- \tfrac{1}{2} \Big[\bar{\Psi}_x \left(\Phi_x P_{\mathrm{R}} + \Phi_{x+\hat{\mu}}^\dagger P_{\mathrm{L}} \right) \Psi_{x+\hat{\mu}} + \bar{\Psi}_x \left(\Phi_x P_{\mathrm{R}} + \Phi_{x-\hat{\mu}}^\dagger P_{\mathrm{L}} \right) \Psi_{x-\hat{\mu}} \Big] \Big\}. \tag{2.4}$$

In both actions the scalar fields $\phi \in \mathrm{Z}(2)$ and $\Phi \in \mathrm{SU}(2)$ are radially frozen and M denotes the fermion matrix. In the case of the SU(2) model the Dirac–fermion fields Ψ_x and $\bar{\Psi}_x$ are SU(2) doublets and $P_{\mathrm{L,R}}$ are the left- and right-handed chiral projectors. There are two kinds of coupling present in both models, namely, the Yukawa coupling and the scalar field hopping term with parameters y and κ,

respectively. In the SU(2) model, in addition, there is a second derivative Yukawa coupling called the Wilson–Yukawa coupling involving the parameter w.

The action in (2.1) and (2.2) is invariant under global chiral $Z(2)_o \otimes Z(2)_e$ transformations

$$\chi \to (\Omega_e P_e + \Omega_o P_o)\chi, \qquad \bar{\chi} \to \bar{\chi}(\Omega_e P_o + \Omega_o P_e), \quad \phi \to \Omega_e \Omega_o \phi, \tag{2.5}$$

where P_e and P_o project onto even and odd sites, respectively,

$$P_{ex} = \tfrac{1}{2}(1 + \varepsilon_x), \qquad P_{ox} = \tfrac{1}{2}(1 - \varepsilon_x), \qquad \varepsilon_x = (-1)^{x_1+x_2+x_3+x_4}, \tag{2.6}$$

and $\Omega_{e,o} = \pm 1$.

In a corresponding manner (e, o $\leftrightarrow$ R, L) the action in (2.3) and (2.4) is invariant under the global chiral $SU(2)_L \otimes SU(2)_R$ transformations

$$\Psi \to (\Omega_L P_L + \Omega_R P_R)\Psi, \qquad \bar{\Psi} \to \bar{\Psi}\big(\Omega_L^\dagger P_R + \Omega_R^\dagger P_L\big), \qquad \Phi \to \Omega_L \Phi \Omega_R^\dagger, \tag{2.7}$$

where $\Omega_{L,R} \in SU(2)_{L,R}$.

The fermionic part of the action for the Z(2) model can be rewritten via a transformation on the fermion fields,

$$\chi'_x = (\phi_x P_{ox} + P_{ex})\chi_x, \qquad \bar{\chi}'_x = \bar{\chi}_x(\phi_x P_{ex} + P_{ox}), \tag{2.8}$$

giving

$$\begin{aligned} S_F &= \bar{\chi}' M' \chi' = \bar{\chi}'\{M'_{\text{off}} + y\,\mathbb{1}\}\chi' \\ &= \sum_{x\mu\pm} \tfrac{1}{2}\eta_{\mu x}\bar{\chi}'_x\Big\{\big(\phi_x \phi_{x\pm\hat{\mu}} P_{ox\pm\hat{\mu}} + P_{ex\pm\hat{\mu}}\big)\chi'_{x\pm\hat{\mu}}\Big\} + y\sum_x \bar{\chi}'_x\chi'_x, \end{aligned} \tag{2.9}$$

where M'_{off} is the off-diagonal part of the fermion matrix M'. Under the above $Z(2)_o \otimes Z(2)_e$ transformations χ' transforms as $\chi' \to \Omega_e \chi'$ and $\bar{\chi}' \to \bar{\chi}' \to \bar{\chi}'\Omega_e$.

Analogous transformations can be performed on the fermion fields in the SU(2) model. When written in terms of the fermion fields

$$\Psi'_x = \big(\Phi_x^\dagger P_L + P_R\big)\Psi_x, \qquad \bar{\Psi}'_x = \bar{\Psi}_x(\Phi_x P_R + P_L), \tag{2.10}$$

which transform as $\mathbb{1}_L \otimes SU(2)_R$, the Yukawa term takes the form of a bare mass term and the Wilson–Yukawa term the form of the standard Wilson mass term familiar from QCD,

$$\begin{aligned} S_F &= \bar{\Psi}' M' \Psi' = \bar{\Psi}'\{M'_{\text{off}} + (y + 4w)\,\mathbb{1}\}\Psi' \\ &= \sum_{x\mu} \tfrac{1}{2}\bar{\Psi}'_x\gamma_\mu\Big\{\big(\Phi_x^\dagger \Phi_{x+\hat{\mu}} P_L + P_R\big)\Psi^\dagger_{x+\hat{\mu}} - \big(\Phi_x^\dagger \Phi_{x-\hat{\mu}} P_L + P_R\big)\Psi'_{x-\hat{\mu}}\Big\} \\ &\quad + y\sum_x \bar{\Psi}'_x\Psi'_x + w\sum_{x\mu}\Big\{\bar{\Psi}'_x\Psi'_x - \tfrac{1}{2}\bar{\Psi}'_x\big(\Psi'_{x+\hat{\mu}} + \Psi'_{x-\hat{\mu}}\big)\Big\}, \end{aligned} \tag{2.11}$$

where M'_{off} again denotes the off-diagonal part of the fermion matrix M'.

An alternative transformation on the fermion fields to, for example

$$\Psi''_x = (\Phi_x P_R + P_L)\Psi_x = \Phi_x \Psi'_x, \qquad \bar{\Psi}''_x = \bar{\Psi}_x(\Phi_x^\dagger P_L + P_R) = \bar{\Psi}'_x \Phi_x^\dagger, \quad (2.12)$$

which transform as $SU(2)_L \otimes \mathbb{1}_R$, corresponds to just a unitary transformation on M' and hence gives the same eigenvalue spectrum. However, note that the Wilson term in the action for the Ψ''_x, $\bar{\Psi}''_x$ fields contains the scalar field in a non-trivial way.

The eigenvalues of M'_{off} are particularly useful in the quenched theory, since they are independent of $y + 4w$ and need only be shifted by $y + 4w$ to give the spectrum of M'. The eigenvalues of M'_{off} and M' can be easily seen to be invariant under $Z(2) \otimes Z(2)$ or $SU(2) \otimes SU(2)$ transformations.

The phase diagrams of the two models are qualitatively quite similar and much is already known about them. In the quenched theory the phase diagram is independent of y (and w for the SU(2) model) and given by the respective pure scalar $Z(2)$ ($\kappa_c = 0.07483(2)$) or $SU(2) \otimes SU(2)/Z(2) \simeq O(4)$ model ($\kappa_c = 0.3045(7)$). There exist a symmetric or paramagnetic phase (PM) ($\kappa_c > \kappa > -\kappa_c$) and two broken phases: a ferromagnetic (FM) phase ($\kappa > \kappa_c$), and an antiferromagnetic (AM) phase ($-\kappa_c > \kappa$).

We illustrate in fig. 1 a schematic phase diagram applicable to either model. For the SU(2) model fig. 1 shows the phase diagram only at $w = 0$. For $w > 0$ the zero of the Yukawa coupling axis is to be shifted in the positive y-direction by an

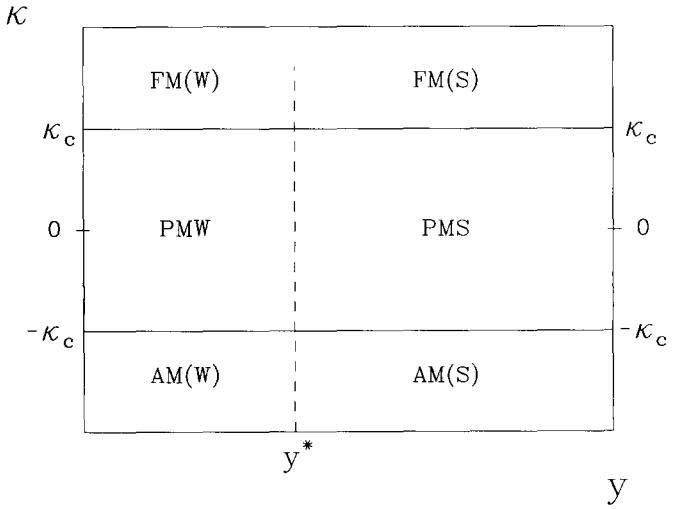

Fig. 1. The schematic phase diagram of either of the models in the quenched approximation. The roughly vertical dashed line at $y = y^*$ represents the crossover. For the Z(2) model $\kappa_c = 0.07483(2)$ and for the $SU(2) \otimes SU(2)$ model $\kappa_c = 0.3045(7)$.

amount of $4w$ [24]. The phases are distinguished by the local order parameters $\langle \Phi \rangle$ (the scalar field vacuum expectation value) and $\langle \Phi_{st} \rangle = \langle (-1)^{(x_1+x_2+x_3+x_4)} \Phi_x \rangle$ (staggered scalar field vacuum expectation value). We use the following abbreviations for the regions of the phases we have found:

Symmetric phases:

PMW: Paramagnetic phase with weak Yukawa couplings:
$\langle \Phi \rangle = \langle \Phi_{st} \rangle = 0$,

PMS: Paramagnetic phase with strong Yukawa couplings:
$\langle \Phi \rangle = \langle \Phi_{st} \rangle = 0$.

Broken symmetry phases:

FM(W): Ferromagnetic phase (weak Yukawa coupling region):
$\langle \Phi \rangle > 0, \quad \langle \Phi_{st} \rangle = 0$,

FM(S): Ferromagnetic phase (strong Yukawa coupling region):
$\langle \Phi \rangle > 0, \quad \langle \Phi_{st} \rangle = 0$,

AM(W): Antiferromagnetic phase (weak Yukawa coupling region):
$\langle \Phi \rangle = 0, \quad \langle \Phi_{st} \rangle > 0$,

AM(S): Antiferromagnetic phase (strong Yukawa coupling region):
$\langle \Phi \rangle = 0, \quad \langle \Phi_{st} \rangle > 0$.

In fig. 1 the FM, the PM and the AM phases are separated by solid lines representing second-order phase transitions. The dashed line approximately parallel to the κ-axis at intermediate values of the Yukawa coupling $y = y^*$ (≈ 1.3–1.4) represents the position of the so-called crossover. In the following we describe briefly the peculiar facts about the crossover. The discussion applies to both of the models. For the SU(2) model the crossover is discussed in the following only at $w = 0$ but can trivially be extended to the $w > 0$ case keeping in mind the shift of the phase diagram for nonzero w.

The FM(W) and FM(S) regions are distinguished by the behaviour of the fermion mass [7,8]. In the FM(W) region the fermion mass m_F decreased as $\kappa \searrow \kappa_c$ for fixed y and w whereas, in the FM(S) region, m_F followed approximately $m_F \approx yz^{-1}$ [16] with $z^2 = \frac{1}{2}\mathrm{Tr}\langle \Phi_x^\dagger \Phi_{x+\hat{\mu}} \rangle$, increasing as $\kappa \searrow \kappa_c$. Associated with this crossover is the technical feature that the number of conjugate gradient iterations N_{CG} required to invert the fermion matrix to a given accuracy showed a maximum in both models at the crossover.

The crossover in the SU(2) model is seen to continue into the symmetric phase, showing little dependence on κ, and splits this phase into two different regions: a massless weak coupling region (PMW) and a strong coupling region (PMS) where the fermions are massive [24]. N_{CG} peaks again around the crossover. The maximum of N_{CG} becomes more pronounced and higher as κ decreased. The observed peak of N_{CG} indicated the presence of the crossover also in the AM phase, though its fate deep in this phase is not known. Similar observations are made in the Z(2) model in this work, and are described at the end of subsect. 4.2.

The correlation of the crossover phenomenon with N_{CG} is not well understood but should be a reflection of the appearance of small eigenvalues in the fermion matrix. This is investigated in detail below. If there appear exactly zero eigenvalues at the crossover, some of the weak and strong regions described above may not be analytically connected and even in the context of the quenched approximation they can be regarded as two distinct phases separated by the crossover.

3. The Lanczos algorithm

We have used the Lanczos method for non-hermitian matrices [25] for calculating the eigenvalues of the Dirac operator M and the related operator M'. In the case of the operator $M^\dagger M$ the simpler hermitian version of this algorithm [26] could be applied. The eigenvalue calculations were performed on independent scalar field configurations which were generated by a simple heat bath algorithm in the case of the Z(2) model and a Hybrid Monte Carlo algorithm in the case of the SU(2) model. The Lanczos algorithm is an iterative algorithm which transforms a given matrix M to a matrix T which has a tridiagonal form,

$$Y^\dagger M X = T, \quad \text{where } Y^\dagger X = \mathbb{1} \text{ and } Y = X \text{ if } M \text{ is hermitian.} \tag{3.1}$$

The transformation matrices $X = (x_1, \ldots, x_N)$ and $Y = (y_1, \ldots, y_N)$ consist of the Lanczos vectors x_i and y_j $(i, j = 1, \ldots, N)$ which are generated iteratively during the process of calculation. If M is non-hermitian it turns out that, because of rounding erros, re-orthogonalization of the above Lanczos vectors is necessary. This requires a large amount of storage space since $2N$ vectors have to be stored simultaneously. The nonzero elements of T are calculated from products of M with these Lanczos vectors. The details of the iterative procedure are described in refs. [25,27]. From the elements of T the eigenvalues can be computed by Sturm sequencing in the case of the hermitian matrix $M^\dagger M$ and by the QL algorithm for the non-hermitian matrices M and M' [27].

4. Eigenvalue distribution in different regions of the phase diagram

We use the non-hermitian version of the Lanczos algorithm described above to find the eigenvalues of M and M'_{off} for the two models. Symmetries exist in both models which can be used to reduce the dimension of the Lanczos vectors.

For the Z(2) model the eigenvalues of M appear in complex conjugate pairs as $\varepsilon M \varepsilon = M^\dagger$ (M is of course real in this model). Since $\varepsilon M'_{\text{off}} \varepsilon = -M'_{\text{off}}$ the eigenvalues of M'_{off} appear in $+/-$ pairs. In addition, because of $\phi M'_{\text{off}} \phi = -(M'_{\text{off}})^\dagger$, the eigenvalues of M'_{off} have the same complex conjugacy symmetry as M.

For the SU(2) model in the absence of a Wilson term the eigenvalues of the fermion matrix M are four-fold degenerate and appear as complex-conjugate pairs. This can be seen by the following. Performing a spin diagonalization [28] replaces the γ-matrices in the hopping term by the site-dependent phase factor $\eta_{\mu x}$. The Yukawa term is unaltered on even sites, but P_L and P_R are interchanged on odd sites. Writing the fermion matrix in this representation in a block form with respect to even/odd sites one can then easily convince oneself that if λ is an eigenvalue, λ^* is also an eigenvalue of this matrix. The four-fold degeneracy is a combination of the two-fold degeneracy arising from the symmetry within the right- and left-handed Dirac subspaces, and another two-fold degeneracy resulting from the pseudo-reality of the SU(2) scalar fields. A similar argument leads to the same symmetry and degeneracy for the eigenvalues of M' and M'_{off}. As in the Z(2) model the eigenvalues of M'_{off} also appear in $+/-$ pairs, because $\gamma_5 M'_{\text{off}} \gamma_5 = -M'_{\text{off}}$, or $\varepsilon M'_{\text{off}} \varepsilon = -M'_{\text{off}}$.

With non-zero Wilson term the generic four-fold degeneracy disappears. The $+/-$ symmetry remains and also the eigenvalues still appear in complex conjugate pairs as can be shown from the pseudo reality of SU(2), charge conjugation and γ_5 transformation.

An important property of M and M' is that their zero modes are related by the transformation (2.8) or (2.10). Note also that their determinants are equal (up to a sign in the Z(2) model), so they vanish simultaneously.

At the beginning it is useful to look at the eigenvalues of the fermion matrix in the limit of the free theory ($\kappa \to \infty$, $\Phi \to \mathbb{1}$). For free Wilson fermions with bare mass y and Wilson parameter w the eigenvalues of the fermion matrix on a hypercubic lattice of volume L^4 are given by

$$y + 4w - w \sum_\mu \cos\, p_\mu \pm i \sqrt{\sum_\mu \sin^2 p_\mu}\,, \tag{4.1}$$

where the allowed momenta with periodic or antiperiodic boundary condition are $p_\mu = 2n\pi/L$ or $p_\mu = (2n+1)\pi/L$, respectively with $n = 0, 1, 2, \ldots, L-1$. For example, the eigenvalues on a 4^4 lattice in the case of naive fermions ($w = 0$) are: y, $y \pm i$, $y \pm \sqrt{2}\,i$, $y \pm \sqrt{3}\,i$ and $y \pm 2i$ (with periodic boundary conditions in all directions) or $y \pm \sqrt{2}\,i$ (with antiperiodic boundary conditions in all directions). In an interacting case the eigenvalue distribution will naturally be different and tend in the limit $\kappa = \infty$ to the free distribution.

However, if one chooses periodic boundary conditions in all directions, real eigenvalues of the free theory at $y = 0$ still appear for the interacting theory in the spectral distribution of M'_{off}. This can be seen as follows. The matrix M'_{off} can be written as $M'_{\text{off}} = M'_{\text{off}}\,(P_L + P_R)$, where $M'_{\text{off}} P_L$ couples to the scalar field and $M'_{\text{off}} P_R$ is free. Hence any eigenfunction of M'_{off} which is purely right-handed will give rise to its corresponding free eigenvalue (and those which are not will have

eigenvalues differing from the free case). In the free theory with periodic boundary conditions in all directions, there are exactly real eigenvalues at 0, $\pm 2w$ and $\pm 4w$, as can be easily seen from eq. (4.1). Their eigenfunctions are also eigenfunctions of γ_5 and hence we can construct eigenfunctions which are purely right- or left-handed. The right-handed modes survive in the interacting theory. In addition, at $w = 0$, $\Phi^\dagger \Psi_{\mathrm{L,free}}$ will be a left-handed eigenvector of M'_{off} with zero eigenvalue if, and only if, $\Psi_{\mathrm{L,free}}$ is a left-handed eigenvector of the free fermion matrix $M(\kappa = \infty)$ at $y = 0$ with zero eigenvalue. Therefore these zero eigenvalues will also remain in the spectra of M'_{off} for all values of κ.

In general at small y periodic boundary conditions in all directions give rise to small eigenvalues which cause strong finite-size effects in various observables and are responsible for the lack of convergence in inversion algorithms of the fermion matrix. For this reason an antiperiodic boundary condition in at least one direction is to be preferred, since then such zero modes do not exist on a finite lattice. On the other hand, with periodic boundary conditions the spectra may appear closer to their form in the infinite lattice limit. Of course, in the infinite lattice limit, the spectral distributions should be independent of the choice of boundary conditions and we therefore change the boundary conditions to get some idea of the strength of finite-size effects.

Because of the technical limitation on the lattice size due to the re-orthogonalization of the Lanczos vectors we cannot perform large-volume calculations with M or M', but in order to get an estimate of the finite-volume effects on the eigenvalue distribution we study the matrices with various boundary conditions for the fermion fields.

In the following we describe the eigenvalue spectra in the different regions of the coupling parameter space for the different models.

4.1. SU(2) MODEL AT $w = 0$

In fig. 2 we show the eigenvalue distribution of the matrices M and M'_{off} for the SU(2) model at $w = 0$ in different regions of the phase diagram. The eigenvalues are in general complex and are represented by the dots in fig. 2 where the abscissae corresponds to the real and the ordinate to the imaginary part. For M the eigenvalue distributions from several independent scalar field configurations are superimposed whereas for M'_{off} we display data for only one configuration. The eigenvalue distribution for the matrix M' is obtained by shifting that of M'_{off} along the positive real axis by y. Since the determinants of the matrices M and M' are equal, the appearance of a zero mode in one should signal its appearance in the other. A similar general description applies also to figs. 3 and 4 to be discussed in subsects. 4.2 and 4.3.

Ferromagnetic phase. Fig. 2a shows the eigenvalue distributions in the FM phase at $\kappa = 0.32$ for M on a 4^4 lattice and for M'_{off} on a 6^4 lattice. In all cases an

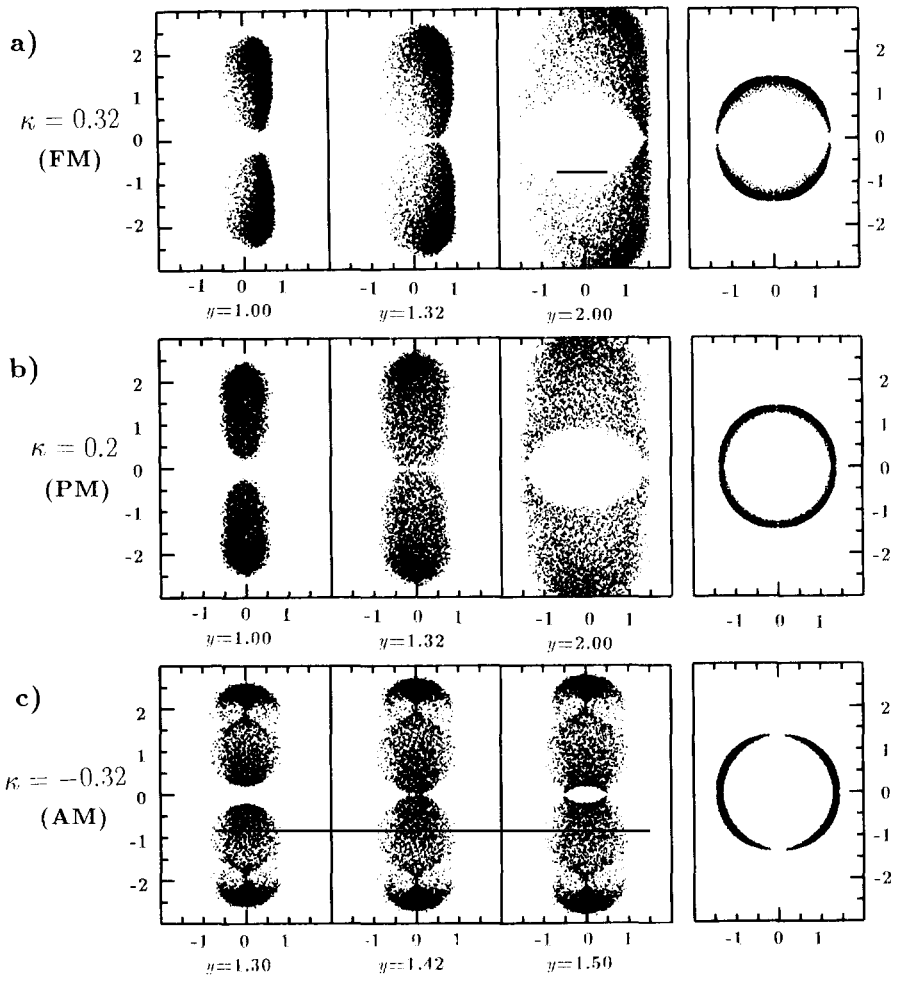

Fig. 2. The eigenvalues of M in nine different regions of the coupling parameter space and the eigenvalues of M'_{off} (right column) in the SU(2)⊗SU(2) fermion–Higgs model at $w = 0$. The plots for M contain 10 configurations on a 4^4 lattice and, for M'_{off}, 1 configuration on a 6^4 lattice. (a) FM phase at $\kappa = 0.32$. The eigenvalues of M are shown (from left to right) at $y = 1.0$, 1.32 and $y = 2.0$ calculated on rotated ϕ-field configurations. Antiperiodic boundary conditions (a.p.b.c.) were imposed only in one direction. (b) PM phase at $\kappa = 0.20$, a.p.b.c. in one direction, the same values of y as in (a). (c) AM phase at $\kappa = -0.32$, a.p.b.c. in all directions, the eigenvalues of M are shown now at $y = 1.30$, 1.42 and $y = 1.50$.

antiperiodic boundary condition in one direction is imposed on the fermion fields. Because of the drift of the scalar field magnetization in the broken phase (no spontaneous symmetry breaking occurs on a finite lattice) we obtain the eigenvalues of M from equilibrated scalar field configurations rotated by an SU(2) ⊗ SU(2) transformation so that the magnetization always points in one predetermined direction. It is easy to see that the eigenvalues of M'_{off} are invariant under such a rotation.

The eigenvalues of M'_{off} nearly form a ring at the chosen value of $\kappa = 0.32$ with no real eigenvalues resulting in a small gap in the ring around the real axis at $\lambda \approx \pm y^*$. But there are eigenvalues very close to the real axis meaning that there will be eigenvalues of M' close to zero when $y = y^*$. The eigenvalues of M at $y = 1.32$ in fig. 2a show also the appearance of small eigenvalues. The crossover region in the FM phase, therefore, shows no exact zero modes but there exist small eigenvalues causing slow convergence of the conjugate gradient algorithm. For $y > y^*$ (strong coupling region) and $y < y^*$ (weak coupling region) the origin lies respectively outside or inside the ring of eigenvalues of M'. Hence small eigenvalues do not appear deep inside these regions as also evidenced by the eigenvalues of M at $y = 1.0$ and $y = 2.0$. As κ increases the gap around the real axis in the M'_{off} distribution grows and in the limit $\kappa \to \infty$ they end up on the imaginary axis with their free values. As $y \to 0$ the eigenvalues of M for any value of κ approach their free values on the imaginary axis.

If periodic boundary conditions are imposed, the shape of the eigenvalue spectrum of M'_{off} remains as shown but with an additional delta function like distribution at the origin due to the free zero modes as described above.

Paramagnetic phase. In the PM phase at $\kappa = 0.2$ (fig. 2b) the eigenvalues of M'_{off} now form a closed ring intersecting the real axis at y^*. This is consistent with the observation that the gap around the real axis vanishes as one approaches the critical line from above. Unlike in the FM phase the matrix M' has zero eigenvalues at $y \approx y^*$. The matrix M in fig. 2b also shows very small eigenvalues at $y = 1.32$. Examination of the distribution of eigenvalues of M'_{off} around the real axis shows approximate real eigenvalues in the range $y = 1.2$–1.4. The density is peaked at the outer edge of the ring.

The appearance of the zero modes as κ decreases through κ_c at y close to y^* is consistent with the observed behaviour of the conjugate gradient algorithm. In this region the number of iterations required to invert the fermion matrix increases dramatically. The algorithm will actually fail to converge if it hits an exact zero mode near y^*. Of course this is very unlikely in practice.

Antiferromagnetic phase. The eigenvalue distribution in the AM phase at $\kappa = -0.32$ is shown in fig. 2c. The same blocking of the fermion matrix M'_{off} as used in deriving the symmetries and degeneracies of its eigenvalues in the beginning of sect. 4 shows that the transformation $\Phi_x \to \varepsilon_x \Phi_x$, which takes $\kappa \to -\kappa$ in the pure O(4) scalar action in eq. (2.3), corresponds to a rotation of 90° in the eigenvalue spectrum. Thus the spectrum at $\kappa = -0.32$ with antiperiodic boundary conditions in one direction can be found by rotating fig. 2a. In fig. 2c we show the spectrum at $\kappa = -0.32$ but with antiperiodic boundary conditions in all directions so that the effect of varying the boundary conditions on M'_{off} in this phase can be seen. Comparing fig. 2a (rotated) with fig. 2c we find no significant difference in the distribution of the eigenvalues of M'_{off} except for a slight shift in the position of the crossover. The eigenvalues of M show that the crossover for antiperiodic boundary

conditions in all directions is around $y = 1.42$ whereas for antiperiodic boundary conditions in only one direction it is around $y = 1.32$.

4.2. Z(2) MODEL

The eigenvalues in the Z(2) model in different regions of the phase diagram are shown in fig. 3. The lattice size is 6^4 for M and 8^4 for M'_{off} with antiperiodic boundary conditions only in one direction in figs. 3a, b and in all directions in fig. 3c. Similar to the SU(2) case, we find small eigenvalues of M and M' at $y = y^* \approx 1.4$. However, this crossover region differs in certain details as described below.

Ferromagnetic phase. The eigenvalue distributions in the FM phase at $\kappa = 0.08$ are shown in fig. 3a. Corresponding to the rotation of the scalar field in the SU(2) model a reflection of the scalar fields $\phi_x \to -\phi_x$ is performed if tunneling occurs. The distribution of M for small eigenvalues shows a structure similar to the SU(2) model in dependence of y. There are also features in the distributions of M'_{off} common to both models, in particular the approximate circular shape close to κ_c. However, in the Z(2) model there is, at this value of κ, no gap around the real axis in the ring of eigenvalues of M'_{off}. Indeed there are exactly real eigenvalues in an interval around 1.4. As a result M' has exact zero eigenvalues at certain values of y in the crossover region. Zero eigenvalues of M have also been detected around $y = 1.4$. This will lead to a lack of convergence of the conjugate gradient algorithm for Yukawa couplings in the region $y \approx 1.2$–1.6, as observed in ref. [7]. However, we find that the width of the interval of real eigenvalues of M'_{off} shrinks from a 4^4 to an 8^4 lattice. At the same time the density of real eigenvalues of M'_{off} does not change appreciably as the volume is increased. Another feature of the M'_{off} spectra in the Z(2) model is the appearance of lines of exactly imaginary eigenvalues even at values of κ very close to κ_c.

Paramagnetic case. The eigenvalue distributions in the PM phase at $\kappa = 0.04$ are shown in fig. 3b. We obtain again a closed circular pattern for M'_{off} as in the SU(2) model. As in the broken phase, the spectrum has lines of real eigenvalues. The width of the crossover does not show a strong volume dependence in this phase, in contrast to the behaviour observed in the broken phase.

Antiferromagnetic phase. In fig. 3c we show the eigenvalue distributions in the AM phase at $\kappa = -0.08$ with antiperiodic boundary conditions in all directions. The M'_{off} distribution implies an appreciable band of y-values around 1.4 for which there exist zero modes of M'. The large width of the crossover region is also seen in the M distribution and this is why examples in the weak and the strong y region in fig. 3c are shown well away from $y = 1.4$, viz. at $y = 0.5$ and $y = 2.0$, respectively.

As $\kappa \to -\infty$ the eigenvalues of M'_{off} for both models must migrate to the real axis, corresponding to the free theory at $\kappa = \infty$ but rotated through 90°. Decreas-

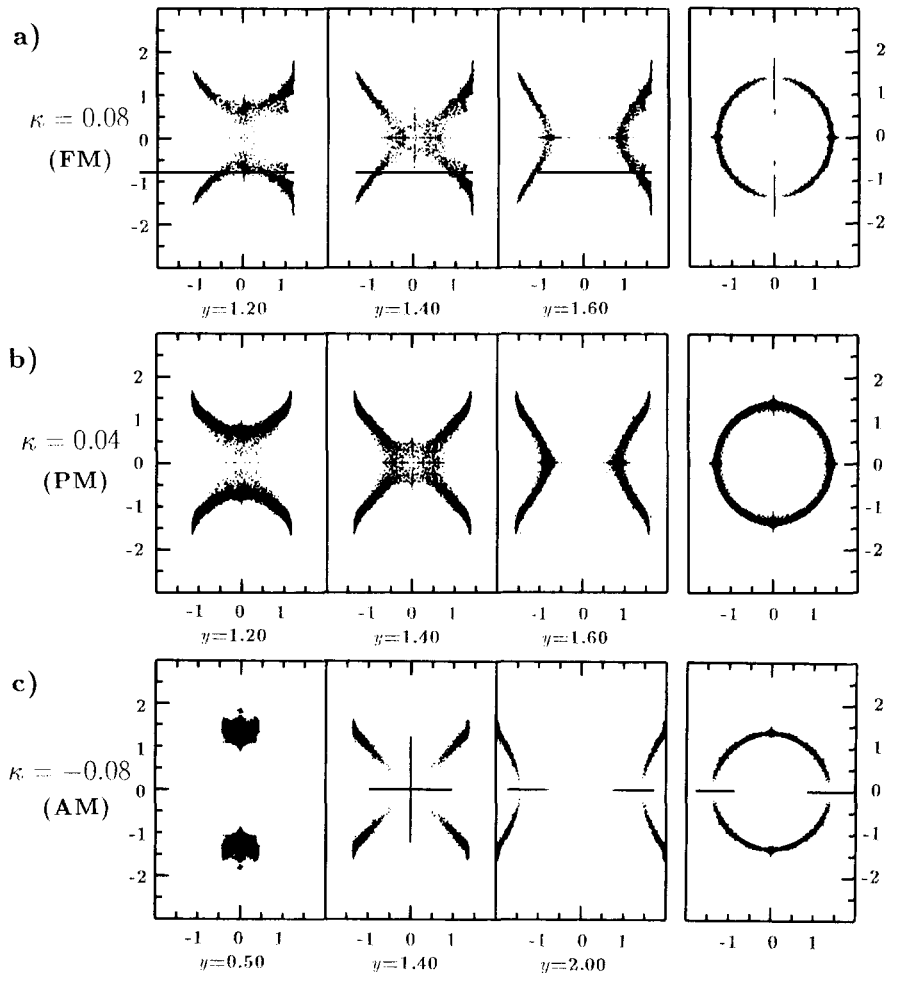

Fig. 3. The eigenvalues of M in nine different regions of the coupling parameter space and the eigenvalues of M'_{off} (right column) in the Z(2)⊗Z(2) fermion–Higgs model. The plots for M contain 5 configurations on a 6^4 lattice and, for M'_{off}, one configuration on a 8^4 lattice. (a) FM phase at $\kappa = 0.08$. The eigenvalues of M are shown (from left to right) at $y = 1.2$, 1.4 and $y = 1.6$ calculated on reflected ϕ-field configurations when tunneling occurs. Antiperiodic boundary conditions (a.p.b.c.) were imposed in one direction only. (b) PM phase at $\kappa = 0.04$, a.p.b.c. in one direction, the same values of y as in (a). (c) AM phase at $\kappa = -0.08$, a.p.b.c. in all directions, the eigenvalues of M are now shown at $y = 0.5$, 1.4 and $y = 2.0$.

ing κ, the circular pattern gradually becomes roughly elliptical, and in the limit $\kappa \to -\infty$ will degenerate to discrete points at $\pm\sqrt{\Sigma_\mu \sin^2 p_\mu}$ dependent on the lattice size and boundary conditions. This is consistent with the observed peaks of the number of conjugate gradient iterations and the poles of the condensate $\langle \bar{\Psi}' \Psi' \rangle$ at the corresponding values of y in the SU(2) model [24].

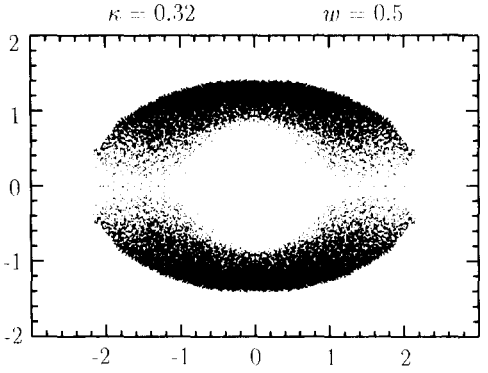

Fig. 4. The eigenvalues of M'_{off} at $\kappa = 0.32$ in the SU(2)⊗SU(2) model with Wilson–Yukawa coupling $w = 0.5$. We display 10 configurations on a 4^4 lattice with antiperiodic boundary conditions only in one direction.

4.3. SU(2) MODEL AT $w > 0$

The spectrum obtained for M'_{off} at $w = 0.5$ in the FM phase at $\kappa = 0.32$ on a 4^4 lattice with antiperiodic boundary condition in one direction is shown in fig. 4. The eigenvalue spectrum of M' is obtained by shifting the spectrum of M'_{off} by $y + 4w = y + 2$. If the M'_{off} spectrum had a width $\leqslant 4$, the origin of the M' spectrum would lie outside the eigenvalue distribution for $y > 0$ consistent with the fact that at $w = 0.5$ the system is in the strong-coupling region for all y. In fact the spectrum is slightly wider than 4 and so, for very small y, zero modes appear leading to bad convergence of the conjugate gradient algorithm. The zero eigenvalues at $y = 0$ is thought to be connected with the criticality of the whole $y = 0$ plane where a fermionic correlation length diverges at any κ in accordance with the Golterman–Petcher symmetry [17]. But the fact that there already appear zero eigenvalues at small values of y is probably due to fluctuations usually expected in small lattices.

We have obtained similar plots at other κ values. There is no significantly different structure in these plots other than the appearance of a gap for $\kappa \gg \kappa_c$. Exactly real eigenvalues appear for $\kappa \approx \kappa_c$ and smaller, but since the model at $w = 0.5$ is in the strong-coupling region the conjugate gradient algorithm should converge except for very small values of y.

5. Volume dependence of the small eigenvalues

As emphasized above, the fact that re-orthogonalization is required to obtain the eigenvalues of M and M'_{off} restricts us to fairly small lattices (up to 8^4 in the Z(2) case). However, to get some idea how the small eigenvalues will behave on

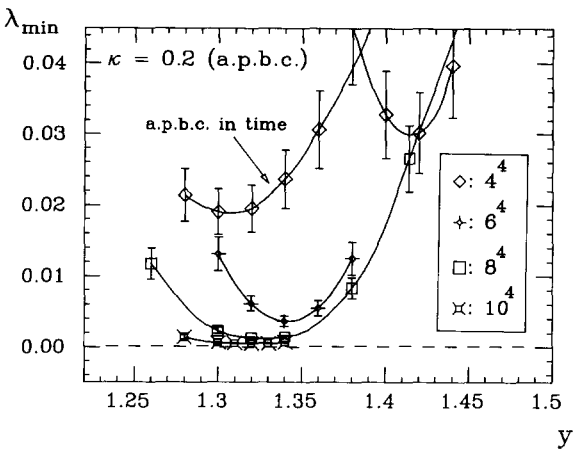

Fig. 5. The y-dependence of the square root of the smallest eigenvalue of $M^{\dagger}M$ for several lattice volumes in the SU(2)⊗SU(2) model in the symmetric phase with antiperiodic boundary conditions in all directions. Also the data obtained from a 4^4 lattice with a.p.b.c. only in one direction are displayed. The eigenvalues were calculated from 10 independent ϕ-field configurations.

larger lattices, we give up the requirement to compute the whole spectrum and study instead the appearance of zero modes. This information can be obtained from the matrix $M^{\dagger}M$ because if $M^{\dagger}M$ has a zero eigenvalue, so has M. Furthermore $M^{\dagger}M$ is hermitian and is therefore more easily diagonalized than M. We use the hermitian Lanczos algorithm on $M^{\dagger}M$ (or on its square root εM in the Z(2) model). This algorithm has the property that the eigenvalues converge in a well-ordered sequence. Usually the large eigenvalues and those close to zero converge first and the algorithm can be stopped once the eigenvalues of interest are obtained. Also no storage of Lanczos vectors is required. Therefore larger lattices can be handled (up to 14^4), but we have to perform computations for each value of y independently.

Fig. 5 shows at $\kappa = 0.2$ and $w = 0$ for the SU(2) model in the PM phase the behaviour of $\lambda_{\min}$, the square root of the smallest eigenvalue of $M^{\dagger}M$, as a function of y on lattices of varying size and with antiperiodic boundary conditions in all directions so that zero modes are inhibited. The data are obtained on lattice sizes ranging from 4^4 to 10^4 and indicate the presence of large finite-size effects. As the volume is increased there are indications that zero eigenvalues exist for a region around y^*. In the Z(2) model measurements on lattices of size up to 14^4 indicate that there is a finite region of y from 1.2 to 1.5 in which there is a non-zero density of zero eigenvalues. In both models, for finite positive values of y significantly smaller than y^*, we find no clear sign of zero modes as the volume is increased. This is in agreement with measurements of the condensate $\langle \bar{\Psi}' \Psi' \rangle$ which is very small in this region as will be discussed in sect. 6.

To show the dependence of the position of the crossover on boundary conditions on small lattices we also display in fig. 5 the behaviour of $\lambda_{\min}$ on a 4^4 lattice

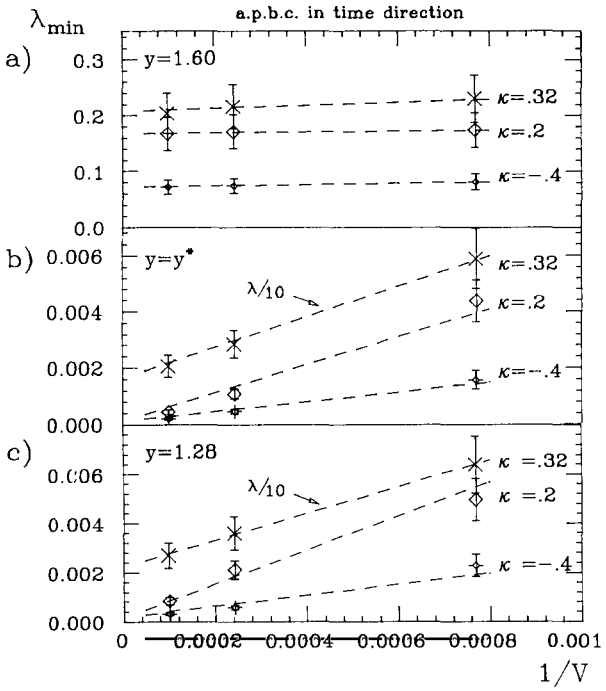

Fig. 6. The volume dependence of the square root of the smallest eigenvalue of $M^{+}M$ in the three different y regions of the coupling parameter space of the SU(2)⊗SU(2) model with antiperiodic boundary conditions in only one direction: (a) strong coupling region; (b) crossover region; (c) y slightly less than y^{*}. The smallest eigenvalues at $\kappa = 0.32$ in (b) and (c) are rescaled by a factor for $1/10$.

with antiperiodic boundary conditions only in one direction. On an 8^4 or larger lattice the minimum of the lowest eigenvalue for the two types of boundary conditions occurs at essentially the same value of y and is, therefore, not shown in this figure.

To elucidate the volume dependence of small eigenvalues, following general wisdom [21,29], we have plotted $\lambda_{\min}$ against $1/V$ in nine different regions. This is shown in fig. 6 for the SU(2) model at $w = 0$. For lattices larger than $V = 4^4$, the data for $\lambda_{\min}$ are consistent with the ansatz of a linear dependence on the inverse lattice volume. In the following we assume the above volume dependence to be also true for volumes larger than the ones (6^4, 8^4, 10^4) used in fig. 6.

In the strong coupling regions of the three phases (fig. 6a) $\lambda_{\min}$, when extrapolated linearly with $1/V$, approaches a non-zero value as the lattice volume goes to infinity. This is consistent with the fact that the origin of the complex plane falls outside of the ring of eigenvalues of M'_{off} in the strong coupling region.

In the crossover region (fig. 6b) we see a marked difference in the extrapolated value of $\lambda_{\min}$ for infinite volume in the FM phase compared to the corresponding

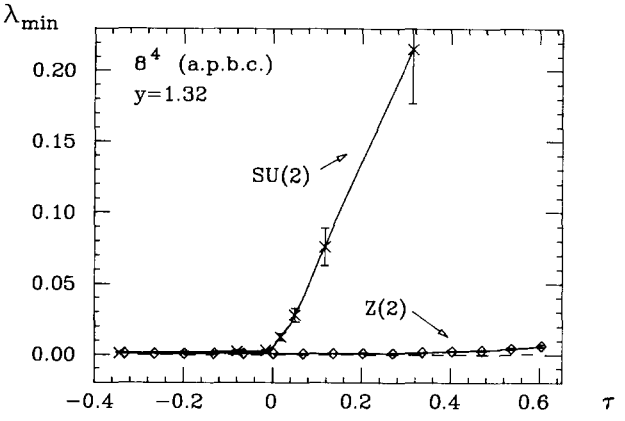

Fig. 7. Dependence of the square root of the smallest eigenvalue of $M^{\dagger}M$ in the crossover region on the reduced temperature $\tau = (\kappa - \kappa_c)/\kappa_c$.

values in the PM and the AM phases. In the former λ_{min} linearly extrapolates to a non-zero value, whereas in the latter phases the extrapolated value is consistent with zero. The different behaviour in the FM phase indicates that the gap which appears around the real axis in M'_{off} distribution for the SU(2) model (fig. 2a) on small lattices will also remain on larger lattices.

The behaviour of λ_{min} at $y = y^*$ continues to y-values somewhat less than y^* in each of the three phases. This is shown for the SU(2) model in fig. 6c. It indicates, as discussed above, that there is a region of y in which zero modes exist in the PM and AM phases.

The same analysis in the case of the Z(2) model shows a similar behaviour of the infinite-volume extrapolation of λ_{min} at the crossover region in the PM and AM phases, whereas in the FM phase it is different. For values of κ somewhat inside the FM phase the scaling curve for λ_{min} at the crossover is still consistent with the extrapolation to zero with the inverse lattice volume. Only quite deep inside the FM region it starts to shy away from zero.

To demonstrate the observed relation between the existence of small eigenvalues at and around the crossover and the scalar phase transition on a given lattice in the two models we show in fig. 7 λ_{min} as a function of the reduced "temperature" $\tau = (\kappa - \kappa_c)/\kappa_c$ at a fixed value of y in the crossover region on an 8^4 lattice. In the SU(2) model the minimum eigenvalue λ_{min} is consistent with zero for $\kappa < \kappa_c$. At $\kappa \approx \kappa_c$ this behaviour changes and for $\kappa > \kappa_c$, λ_{min} increases monotonically with κ. In contrast there is no sharp change in the behaviour of λ_{min} at $\kappa \approx \kappa_c$ in the Z(2) model, also shown in fig. 7. There the appearance of small eigenvalues continues in the FM phase and λ_{min} starts to increase very slowly deep in the FM phase.

An analysis of the spectral density $\rho(\lambda_{\min})$ at the crossover at $\kappa = 0.2$, i.e. in the PM phase of the SU(2) model shows, similar to the findings of refs. [21,22], that $\rho(\lambda_{\min})$ is nearly independent of volume for the investigated range from 6^4 to 10^4. Similar results emerge also in the PM and part of the FM phase for the Z(2) model at the crossover.

6. Fermion condensates

Fermion condensates on our finite lattices can be readily calculated from the eigenvalues of the fermion matrices M and M'_{off}. They agreed very well with the condensate values calculated using other methods, for example, the noisy estimator method [30]. In the following we discuss the fermion condensates of the SU(2) model at $w = 0$ specifically in the PM phase. A similar discussion applies in general also for the Z(2) model.

As must happen in the PM phase, the symmetry of the M spectra requires for all values of y a vanishing $\langle \bar{\Psi}\Psi \rangle$ given by

$$\langle \bar{\Psi}\Psi \rangle = \frac{1}{8V} \sum \frac{1}{\lambda}, \tag{6.1}$$

where the sum extends over all the eigenvalues λ of M.

In the PM phase it is more interesting to consider, from the eigenvalues of M'_{off}, the y-dependence of the condensate

$$\langle \bar{\Psi}'\Psi' \rangle = \left\langle \bar{\Psi}\left(\Phi P_{\text{R}} + \Phi^{\dagger} P_{\text{L}}\right)\Psi \right\rangle = \frac{1}{8V} \sum \frac{1}{\lambda'_{\text{off}} + y}, \tag{6.2}$$

where the sum extends over all the eigenvalues λ'_{off} of M'_{off}. Please note that one gets the whole y-dependence from only one set of eigenvalues λ'_{off} at $y = 0$. The condensate $\langle \bar{\Psi}'\Psi' \rangle$ in contrast to $\langle \bar{\Psi}\Psi \rangle$, is invariant under the global $\text{SU(2)}_{\text{L}} \otimes \text{SU(2)}_{\text{R}}$ transformations and therefore does not have to vanish in the symmetric phase. Since from the discussion of sects. 4 and 5 there is enough indication that fermionic observables in the strong and weak regions of the PM phase are not analytically connected through the crossover at $y = y^*$ where there seem to appear zero eigenvalues in the thermodynamic limit, the calculation of the invariant condensate as a function of y is particularly relevant there.

To have a better intuition of the y-dependence of this condensate the following analogy with two-dimensional electrostatics is useful. The condensate is given by the electric field as would be produced at the origin by a distribution of negative unit charges exactly in the place of the eigenvalues of M'. The closed ring structure of the eigenvalue distribution (which looks almost uniform) of M'

immediately indicates that $\langle \bar{\Psi}'\Psi' \rangle$ is zero for all $y < y^*$, whereas at $y > y^*$ $\langle \bar{\Psi}'\Psi' \rangle$ is non-zero and decreases as $1/y$ due to the Gauss law in two-dimensional electrostatics. We have actually calculated the primed condensate according to eq. (6.2) and indeed find it to be very small in the weak coupling region growing quite suddenly at the crossover and then falling off as $1/y$ in the strong coupling region. In a previous paper [24] we have shown fermion masses to be consistent with zero in the PMW phase whereas fermions are massive in the PMS phase.

7. Fermion masses

Fermion masses are to be derived from the large-distance behaviour of the fermion propagator. Nevertheless, let us consider the following simple-minded exercise. Let us try to estimate an effective free fermion mass parameter m from the eigenvalue distribution by comparing the fermion condensate as obtained from the eigenvalues to that of a free fermion. This is of course not a valid procedure in general for determining the fermion mass since the condensate is a local observable and will also have contribution from all higher states.

Let us consider the eigenvalues of the scalar–fermion theory and of the free theory only in the upper half of the complex plane of eigenvalues and compute the complex condensates in the interacting and the free theories and match them on the same sized lattice and with the same boundary conditions, i.e.

$$\langle \bar{\Psi}\Psi \rangle = Z \langle \bar{\Psi}\Psi \rangle_{\text{free}}, \tag{7.1}$$

where Z is a real normalization constant and the condensates are obtained from their associated eigenvalues only with positive imaginary parts. If exact real eigenvalues appear, only half of them are taken into account. In the SU(2) model we then estimate the effective free fermion mass parameter m by making a choice for the effective Wilson parameter r and solving the equation

$$\frac{\mathrm{Re}\left[\langle \bar{\Psi}\Psi \rangle(\kappa, y, w)\right]}{\mathrm{Im}\left[\langle \bar{\Psi}\Psi \rangle(\kappa, y, w)\right]} = \frac{\mathrm{Re}\left[\langle \bar{\Psi}\Psi \rangle_{\text{free}}(m, r)\right]}{\mathrm{Im}\left[\langle \bar{\Psi}\Psi \rangle_{\text{free}}(m, r)\right]} = \frac{\sum_p \dfrac{m + 4r - rc}{(m + 4r - rc)^2 + s^2}}{\sum_p \dfrac{-s}{(m + 4r - rc)^2 + s^2}}, \tag{7.2}$$

where $s = \sqrt{\Sigma_\mu \sin^2}$ and $c = \Sigma_\mu \cos p_\mu$. In the Z(2) model the same equation is applicable, but of course with $r = 0$. In the trivial case of a free fermion with mass m_{F} the parameter m would of course be equal to m_{F}.

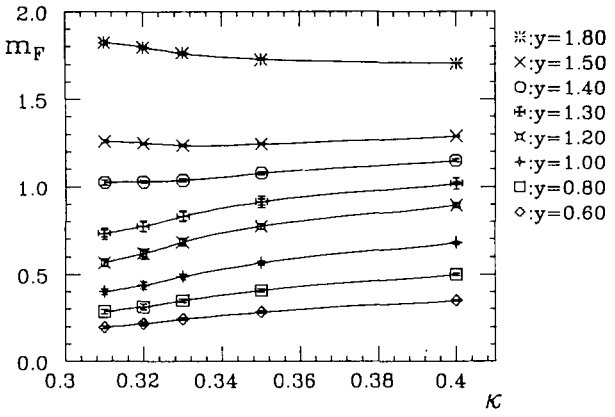

Fig. 8. The condensate mass on a 4^4 lattice for the SU(2)⊗SU(2) model as a function of κ for different values of y around y^*.

We have used this definition to estimate m from the condensate $\langle \bar{\Psi}'\Psi' \rangle$ since its associated spectrum is Z(2) ⊗ Z(2) or SU(2) ⊗ SU(2) invariant. Also, M'_{off} is independent of y and hence we can obtain in the quenched theory the y-dependence of m from the set of eigenvalues at a chosen κ. The κ-dependence of m estimated this way is shown in fig. 8 for the SU(2) model at $w = 0$ (for which of course $r = 0$) for various values of y in the broken phase. The parameter m reflects the same qualitative behaviour as the renormalized fermion mass: for $y < y^*$ it decreases as $\kappa \searrow \kappa_c$, whereas it increases for $y > y^*$ [8].

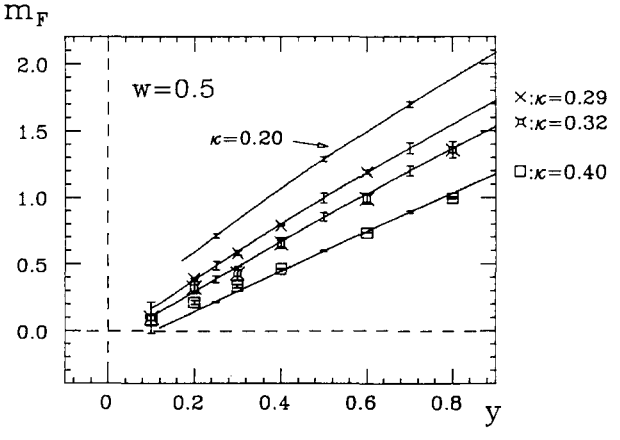

Fig. 9. The condensate mass and the propagator mass as a function of y at $w = 0.5$ for several values of κ in the SU(2)⊗SU(2) model. The propagator masses are calculated on a $6^3 \times 12$ lattice (symbols) and the condensate masses are obtained on a 4^4 lattice (lines). Representative error bars for the condensate mass are displayed for three y-values.

The estimate of m with Wilson fermions requires knowledge of r. We take the ad hoc choice $r = w$ which is reasonable in the vicinity of the crossover [11]. Fig. 9 shows the parameter m (lines) and the propagator mass (symbols) as a function of y for fixed values of κ at $w = 0.5$ in the FM and PM phases. There is remarkable agreement between the two observables. For small values of y we enter a region where zero eigenvalues appear in the spectrum of M' (see fig. 4), making mass estimates unreliable.

We find it surprising that the mass estimate from fermion condensates has the correct qualitative behaviour. It indicates that the fermion propagators in our system are quite close to free propagators at all distances.

8. Summary and outlook

The analysis of the eigenvalue spectra of the operators M, $M^\dagger M$ and M' provides additional insight into the phase structure of the Z(2) ⊗ Z(2) and SU(2) ⊗ SU(2) fermion–Higgs models. In many previous publications the authors reported on the bad convergence properties of the conjugate algorithm around the crossover line in the FM and PM phases. The analysis of the eigenvalue spectra shows that this problem is caused by the appearance of small eigenvalues around the crossover line.

Assuming that our extrapolation ansatz for $\lambda_{\min}$ is correct upto infinite volume and the spectral density does not depend strongly on the volume as we find it in the range of our investigated volumes, we can also make statements about the thermodynamic limit, namely that there exist zero eigenvalues at the crossover in the PM phase even in this limit. The PM phase then is separated into two distinct phases PMW and PMS. In the Z(2) model the line of zero eigenvalues in the PM phase seems even to continue some distance into the FM phase while in the SU(2) model at the crossover in the FM phase there exist small eigenvalues, but not exactly zero eigenvalues in the thermodynamic limit.

An effective free fermion mass parameter extracted from the fermion condensate has, interestingly, correct qualitative behaviour and points out that the fermion propagators in these systems probably resemble quite well the free propagators at all distances.

The results summarized above are obtained from the quenched version of the theory. Inclusion of the fermion determinant in the simulations must modify these conclusions, since configurations with small eigenvalues will be suppressed. The extension of the analysis to the full dynamical theory has been discussed for QCD [31] and can be extended to the two models discussed above. For both of these models, the partition function can be written as a polynomial in the Yukawa coupling whose coefficients are determined from the eigenvalues of the fermion

matrix M'_{off}. The complex zeros of this polynomial, in particular those closest to the real axis, determine the physical properties of the model like e.g. the phase structure and the critical exponents. Furthermore, the knowledge of the coefficients of the polynomial allows one to calculate, from the partition function, thermodynamic quantities as functions of the Yukawa coupling. An investigation of the complex zeros and their scaling behaviour with respect to lattice volume is underway for the $Z(2) \otimes Z(2)$ model. Of course one expects differences between the phase structure of the quenched theory and that of the dynamical theory. But the question is whether such differences change most of the conclusions in this paper qualitatively.

One solid conclusion of this investigation in the quenched approximation, that the two PM regions PMW and PMS are to be regarded as two distinct phases, remain unchanged as the phase diagram with dynamical fermions [24] reveal them to be really separate phases. The advantage of knowing e.g. that PMS is a phase distinct from PMW even in the quenched approximation has several conveniences. Much of the success of the approach to chiral gauge theories on the lattice using the so-called Wilson–Yukawa coupling seems to depend crucially on the results of several precision measurements in the PMS phase [13] and these can be performed with moderate resources in the quenched approximation. Our findings in this paper make these measurements in the PMS phase meaningful.

The significance of the PMS phase is not clear. As has been pointed out in sect. 1, with usual Yukawa couplings only, this is a phase where all the fermions decouple in the continuum limit leaving a pure scalar theory. With the introduction of the chiral-invariant Wilson–Yukawa coupling, the PMS phase seems natural for the construction of asymptotically free chiral gauge theories [9] because the doublers apparently can be decoupled there satisfactorily [13]. On the other hand, there exist, in the PMS phase, massive Dirac fermions [13]. The scaling properties of these fermion masses are not convincingly known. It is not yet clear what kind of a theory would finally emerge in any of the strong regions, especially in the PMS phase. These issues, discussed quite comprehensively in ref. [18], are being investigated at the moment.

A part of the results presented in this paper has already been reported in ref. [32].

We have benefitted from discussions with J. Jersák, R. Shrock and J. Shigemitsu. The continuous support by H.A. Kastrup is gratefully acknowledged. The computations on the SU(2) model were performed on the CRAY Y-MP/832 at HLRZ Jülich. The computations on the Z(2) model were performed at the Rutherford Laboratory on the IBM 3090/600E with support from IBM and the CRAY X-MP under grant CR/G 0095.2 from the UK SERC. C.T.H.D. is grateful for an SERC Advanced Fellowship and D.H. for an SERC studentship.

References

[1] P. Hasenfratz, Nucl. Phys. B (Proc. Suppl.) 9 (1989) 3
[2] D.J.E. Callaway, Phys. Rep. 167 (1988) 241
[3] J. Jersák, *in* Higgs particle(s) – Physics issues and searches in high energy collisions, Erice, 1989, ed. A. Ali (Plenum, New York, 1990) p. 39
[4] J. Kuti, Nucl. Phys. B (Proc. Suppl.) 9 (1989) 55
[5] H. Neuberger, Nucl. Phys. B (Proc. Suppl.) 17 (1990) 17
[6] J. Shigemitsu, Nucl. Phys. B (Proc. Suppl.) 20 (1990) 515
[7] A. Hasenfratz and T. Neuhaus, Phys. Lett. B220 (1989) 435;
A. Hasenfratz, Lattice Higgs Workshop, ed. B. Berg et al. (World Scientific, Singapore, 1988) p. 229
[8] W. Bock, A.K. De, K. Jansen, J. Jersák and T. Neuhaus, Phys. Lett. B231 (1989) 283
[9] J. Smit, Nucl. Phys. B (Proc. Suppl.) 17 (1990) 3
[10] J. Smit, Acta Phys. Pol. B17 (1986) 531 [Zakopane 1985]; Nucl. Phys. B175 (1980) 307; Nucl. Phys. B (Proc. Suppl.) 4 (1988) 451;
L.H. Karsten, Field theoretical methods in particle physics, ed. W. Rühl (Plenum, New York, 1980);
P.D.V. Swift, Phys. Lett. B145 (1984) 256
[11] W. Bock, A.K. De, K. Jansen, J. Jersák, T. Neuhaus and J. Smit, Phys. Lett. B232 (1989) 486;
A.K. De, Nucl. Phys. B (Proc. Suppl.) 17 (1990) 484
[12] W. Bock and A.K. De, Phys. Lett. B245 (1990) 207;
W. Bock, Nucl. Phys. B (Proc. Suppl.) 20 (1991) 559
[13] A.K. De, Nucl. Phys. B (Proc. Suppl.) 20 (1991) 572;
W. Bock, A.K. De and J. Smit, HLRZ 91-81
[14] A.M. Thornton, Phys. Lett. B227 (1989) 434
[15] S. Aoki, I.-H. Lee, J. Shigemitsu and R.E. Shrock, Phys. Lett. B243 (1990) 403
[16] J. Smit, Nucl. Phys. B (Proc. Suppl.) 9 (1989) 579
[17] M.F.L. Golterman and D.N. Petcher, Phys. Lett. B225 (1989) 159; B247 (1990) 370
[18] M.F.L. Golterman, Nucl. Phys. B (Proc. Suppl.) 20 (1990) 528
[19] R. Setoodeh, C.T.H. Davies and I.M. Barbour, Phys. Lett. B213 (1988) 195
[20] G. Salina and A. Vladikas, Nucl. Phys. B (Proc. Suppl.) 17 (1990) 365
[21] S. Hands and M. Teper, Nucl. Phys. B 347 (1990) 819
[22] S. Hands, J. Kogut and E. Dagotto, Nucl. Phys. B333 (1990) 551;
M. Göckeler, R. Horsley, E. Laermann, P. Rakow, G. Schierholz, R. Sommer and U.-J. Weise, Nucl. Phys. B334 (1990) 527
[23] J. Smit and J.C. Vink, Nucl. Phys. B286 (1987) 485; B303 (1988) 36;
J.C. Vink, Nucl. Phys. B307 (1988) 549
[24] W. Bock, A.K. De, J. Jersák, K. Jansen, T. Neuhaus and J. Smit, Nucl. Phys. B344 (1990) 207
[25] I.M. Barbour, N.-E. Behilil, P.E. Gibbs, G. Schierholz and M. Teper, The recursion method and its applications, ed. D.G. Pettifor and D.L. Weaire (Springer, Berlin, 1985).
[26] C. Lanczos, J. Res. Nat. Bur. Stand. 45 (1952) 409
[27] I.M. Barbour and C.T.H. Davies, in preparation;
J. Cullum and R.A. Willoughby, Sparse Matrix Proceedings 1978, ed. I.S. Duff and G.W. Stewart (SIAM, Philadelphia, PA, 1979)
[28] N. Kawamoto and J. Smit, Nucl. Phys. B192 (1981) 100
[29] T. Jolicoeur and A. Morel, Nucl. Phys. B262 (1985) 627;
J. Gasser and H. Leutwyler, Phys. Lett. B188 (1987) 477
[30] K. Bitar, A.D. Kennedy, R. Horseley, S. Meyer and P. Rossi, Nucl. Phys. B313 (1989) 348
[31] I.M. Barbour and A.J. Bell, Glasgow University preprint GUTPA/91/5-2
[32] C.T.H. Davies, Nucl. Phys. B (Proc. Suppl.) 20 (1991) 568